Transp Porous Med (2012) 93:815–829
DOI 10.1007/s11242-012-9985-0

The Effective Permeability of Cracks and Interfaces in Porous Media

Franck J. Vernerey

Received: 7 October 2011 / Accepted: 7 March 2012 / Published online: 22 March 2012

Abstract The presence of interfaces in fluid/solid biphasic media is known to strongly influence their behavior both in terms of solid deformation and fluids flow. Mathematical models have traditionally represented these interfaces as lines of no-thickness and whose behavior is given in terms of effective permeabilities whose physical meaning is often disconnected to the microscopic nature of the interface. This article aims to reconcile macroscopic and microscopic interface representations by investigating how the nature of microscopic flows and pressures in the interface can be used to explain its macroscopic behavior. By invoking a proper thickness average operation, we derive an closed form expression that relates the effective interfaces permeabilities to its microscopic properties. In particular, we find that the effective interface permeabilities are strongly influenced by three factors: the ratio of bulk and interface permeabilities, the fluid viscosity, and the physical thickness of the interface.

Keywords Effective permeability · Porous interface · Darcy–Brinkman law

1 Introduction

The mechanics of fluid flow in porous media is a key phenomenon in a variety of engineering applications ranging from soil mechanics to construction materials. More recently, it has also found a wide range of biomedical applications due to the hydrated nature of biological media such as soft-tissues, hydrogels, (Vernerey et al. 2011b) and biological cells (Vernerey and Farsad 2011a; Vernerey et al. 2011a). The theory of porous media, originally introduced by Biot (1941, 1957) in the context of consolidation and later generalized to the theory of mixtures, notably by Truesdell and Bowen (Bowen 1980; Truesdell 1999) has been very successful at describing the interactions between fluid flow and biphasic solid deformation.

F. J. Vernerey (✉)
Department of Civil, Environmental and Architectural Engineering, University of Colorado, Boulder, CO, USA
e-mail: franck.vernerey@colorado.edu

However, as any continuum theories, mixture formulations are not readily appropriate for describing discontinuous fields originating from the presence of interfaces (such as cracks or embedded membranes) within a material's microstructures. This represents a challenge since such discontinuities may critically affect the nature of the interstitial fluid flow as well as the elastic deformations. Various strategies have therefore been elaborated to address this issue, with a particular interest on describing fluid flow in a fractured porous media (Barthelemym 2009; Liolios and Exadaktylos 2008; Pouya and Ghabezloo 2008; Ghabezloo and Pouya 2008). In the case where interfaces are cracks, fluid flow has traditionally been described by a Poiseuille-type distribution that can be determined by carefully handling boundary conditions between the free fluid flow in the interface and that in the surrounding porous medium (Chandesris and Jamet 2006; Goyeaua et al. 2003). These methods particularly enabled the derivation of useful relationships between effective permeability and internal crack structure. With the same objective in mind, different approaches have later been introduced. For instance, one approach consisted in describing cracks as thin ellipsoidal inclusions for which an effective permeability could be derived using self-consistent homogenization techniques (Dormieux and Kondo 2007; Barthelemym 2009). Similarly, Lolios and Exadaktylos (2008) and later Pouya and Ghabezloo (2008), described cracks as lines of pressure discontinuity that could subsequently be used to determine the interfacial fluid flow. We note that while the above studies were extremely useful in estimating the effective permeability of microcracked porous media, they did not consider the case of a porous material interfaces nor did they consider the coupling between solid deformation and interface flow.

To tackle these shortcomings, we have recently introduced a general theory (Vernerey 2011) that can describe the combined deformation and fluid flow in an elastic porous medium with interfaces. Due to its flexibility, the formulation is able to characterize a variety of phenomena including both interface deformation (Gurtin et al. 1998), surface tension (Farsad et al. 2010; Vernerey and Farsad 2011b) as well as interface fluid flow and its coupling with elastic deformations. However, as it is based on macroscopic assumptions, the theory does not specify the links between constitutive relation and the nature of the underlying structure of the medium which, as a consequence, precludes any applications to real materials and interfaces. This article addresses this issue by presenting an analytical analysis of fluid flow in a porous interface in order to provide a clear link between macroscopic interface permeabilities and the microscopic nature of the interface it represents (including the thickness, permeability, effective viscosity of the interface, as well as those of its surrounding medium). To reconcile macroscopic and microscopic interface descriptions, we first determine an expression for interface flows when macroscopic pressure gradients are present by solving the Darcy–Brinkman equation in the interface neighborhood. Upon obtaining the solution, the concept of thickness averaging introduced in our earlier work (Vernerey 2011) is invoked in order to compute effective interface permeabilities in terms of interface and bulk properties. Besides obtaining useful relationships relating macro- and microscopic interface descriptions, the present analysis provides an interesting insight, both qualitatively and quantitatively, onto the nature of fluid flow in interfaces whose properties may drastically differ from that of the surrounding medium.

This article is organized as follows. In the next section, we provide a short summary of the theoretical framework used to model fluid flow in porous media with thin interfaces. In Sect. 3, we concentrate on the microscopic view of the interface and derive expressions for the normal and tangential flow across an interface of finite thickness, when subjected to macroscopic pressure gradients. The results are then used in Sect. 4 to determine key relationships between macroscopic permeabilities and interface properties and concluding

Table 1 Nomenclature

Definition	Symbol	Unit
Symbols and notations		
Average of macroscopic fields across interface	$\{\}$	n/a
Jump in macroscopic fields across interface	$[\,]$	n/a
component of continuum fields normal to interface	Superscript $\perp$	n/a
component of continuum fields tangential to interface	Superscript $\parallel$	n/a
Porosities		
Bulk porosity	ϕ	n/a
Mean interface porosity	$\bar{\phi}$	n/a
Permeabilities		
Bulk permeability	$\boldsymbol{\kappa}^{\mathrm{B}}$	m^2
Microscopic interface permeability	$\boldsymbol{\kappa}^{I}$	m^2
Mean interface permeability (normal and tangential)	$\boldsymbol{\kappa}_s^{\perp}$ $\boldsymbol{\kappa}_s^{\parallel}$	m^2
Interface permeability to $\mathbf{q}_m$ (normal and tangential)	$\boldsymbol{\kappa}_m^{\perp}$ $\boldsymbol{\kappa}_m^{\parallel}$	m^2
Viscosities		
Dynamic viscosity of interstitial fluid	μ	Pa s
Effective Brinkman viscosity in the bulk and in interface	μ^{B} and μ^{I}	Pa s
Velocities		
Fluid velocity in the bulk	$\mathbf{q}$	m/s
Mean interface velocities (total, normal, and tangential)	$\mathbf{q}_s$, $q_s^{\perp}$, and, $\mathbf{q}_s^{\parallel}$	m/s
First moment of interface velocity (total, normal, and tangential)	$\mathbf{q}_m$, $q_m^{\perp}$, and, $\mathbf{q}_m^{\parallel}$	m/s
Pressure and dimension		
Fluid pressure	p	Pa
Interface thickness	$2h$	m

remarks are provided in Sect. 5. The notations and nomenclature used in the manuscript are summarized in Table 1.

2 Incompressible Fluid Flow in Porous Media with Interfaces

Let us consider a three-dimensional porous solid defined in a domain Ω and delimited by a boundary $\partial\Omega$. Within this domain, we consider the existence of thin curved interfaces that may be viewed as two-dimensional surfaces Γ whose orientation is defined by the unit vector $\mathbf{n}$ normal to the plane tangent to Γ locally (Fig. 1). At the microscopic level, however, interface are seen as material layers of finite thickness $2h$ filled with a porous medium, assumed to be perfectly bounded by the surrounding bulk material.

We now wish to describe the phenomena responsible for fluid flow in both bulk and interface. Generally, such flows may result from a variety of phenomena including the presence of pressure gradients or electrical fields, as well as the presence of gravitational force that may be united into a global potential function ψ (Sun et al. 1999) such that fluid velocity $\mathbf{q}$ in the bulk can be written:

$$\mathbf{q} = -\frac{\boldsymbol{\kappa}}{\mu}\nabla\psi, \tag{1}$$

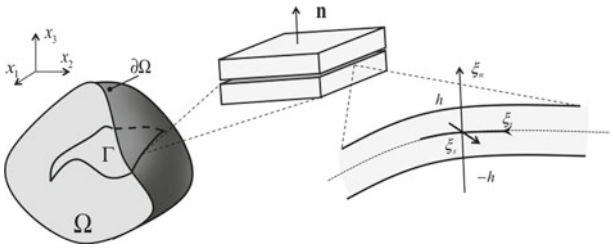

Fig. 1 Porous solid Ω containing interfaces Γ and the normal vector to interfaces

where $\boldsymbol{\kappa}$ is the permeability tensor, and μ is the fluid's dynamic viscosity. Concentrating on pressure-driven flows, the potential function becomes $\psi = p$ (p denoting the fluid pressure) and (1) takes the conventional form of Darcy's law.

2.1 Interface fluid driving forces and flows

As discussed above, when interfaces are present, the pressure field p (and its gradient) may not always be continuous across Γ and the interstitial fluid flow cannot be simply described by (1). As discussed in Vernerey (2011), pressure gradients and discontinuities across Γ may be captured by the following four quantities:

$$[p] \quad \{\nabla p\}^{\parallel} \quad [\nabla p]^{\perp} \quad [\nabla p]^{\parallel}, \tag{2}$$

where $[\cdot]$ stands for a jump in the enclosed quantity, while $\{\cdot\}$ denotes an average of the enclosed quantities on both side of the interface. In addition, the superscripts $\parallel$ and $\perp$ are scalar quantities denoting the tangential and normal projection of a vector $\mathbf{v}$ on the interface according to:

$$v^{\parallel} = \|\mathbf{P}^{\parallel}\mathbf{v}\| \quad \text{and} \quad v^{\perp} = \mathbf{v}\cdot\mathbf{n}, \tag{3}$$

where the symbol $\|\cdot\|$ denotes the L_2 norm of a vector. In addition, the tangential projection operator is defined by $\mathbf{P}^{\parallel} = \mathbf{I} - \mathbf{n}\otimes\mathbf{n}$ where the symbol $\otimes$ denotes the dyadic product and $\mathbf{I}$ is the second-order identity tensor. The four quantities in (2) may be thought of as driving forces for the following four conjugate interface velocities:

$$q_s^{\perp} \quad q_s^{\parallel} \quad q_m^{\perp} \quad q_m^{\parallel}. \tag{4}$$

Here, the first two terms describe the normal and tangential mean velocities through the interface, while the last two terms denote the normal and tangential components of the first moment of the interface velocity distribution, respectively (Fig. 2). A more precise definition of these variables is given later in the manuscript (Eq. (16)).

2.2 Mass conservation

Macroscopic equations governing fluid flow in a porous medium with interfaces are then written in terms of two sets of equations: (1) mass conservation and (2) a constitutive relation relating fluid fluxes and their associated driving forces. Considering the case of an incompressible fluid (the more general case of compressible fluids is discussed in Vernerey 2011), mass conservation in the bulk yields:

$$\operatorname{div}(\phi\mathbf{q}) = 0, \tag{5}$$

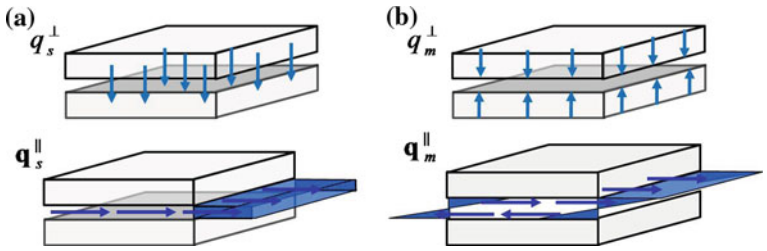

Fig. 2 Illustration of normal and tangential fluid velocities in the interface

where ϕ is a scalar quantity describing the bulk porosity. Moreover, considering an interface with constant porosity $\bar{\phi}$, mass conservation in Γ was shown to take the following form for an incompressible fluid:

$$\mathrm{div}^{\parallel}\left(\bar{\phi}\mathbf{q}_s^{\parallel}\right) + \frac{[\phi\mathbf{q}\cdot\mathbf{n}]}{2h} = 0 \tag{6}$$

$$\mathrm{div}^{\parallel}\left(\bar{\phi}\mathbf{q}_m^{\parallel}\right) + \frac{1}{2Ih}\left(\{\phi\mathbf{q}\cdot\mathbf{n}\} - \bar{\phi}q_s^{\perp}\right) = 0, \tag{7}$$

where $\mathbf{q}_s^{\parallel} = q_s^{\parallel}\mathbf{t}$ and $\mathbf{q}_m^{\parallel} = q_m^{\parallel}\mathbf{t}$ are the tangential interface velocity vectors whose direction is given by the unit tangential vector $\mathbf{t}$ to the interface. Moreover, the symbol $\mathrm{div}^{\parallel}$ denotes the surface divergence operator, and I is a moment of inertia-like quantity defined as:

$$I = \frac{1}{(2h)^3}\int_{-h}^{h}\xi_n^2 \mathrm{d}\xi_n = \frac{1}{12}. \tag{8}$$

Equation (6) describes how tangential velocities are affected by the amount of fluid coming from the bulk into the interface (or vice versa). Similarly, Eq. (7) represents the mass balance in terms of $\mathbf{q}_m^{\parallel}$ and the average normal velocity $\mathbf{q}\cdot\mathbf{n}$ passing though the interface. The above equations therefore naturally describe the coupling between fluid flow in the bulk and interface.

2.3 Constitutive assumptions

Traditionally, the steady flow of a fluid through a porous medium has been described by Darcy's law in the form shown in (1). However, when interfaces are present, significant fluid velocity gradients may develop in the vicinity of the interface, giving rise to boundary layers. The characteristic length-scale of the boundary layers is very sensitive to the fluid viscosity, a phenomenon that is well captured by the Darcy–Brinkman equation:

$$\mathbf{q} = \frac{\kappa^{\mathrm{B}}}{\mu}\left(-\nabla p + \mu_{\mathrm{e}}^{\mathrm{B}}\nabla^2\mathbf{q}\right), \tag{9}$$

where $\mu_{\mathrm{e}}^{\mathrm{B}}$ is the effective Brinkman viscosity, and κ^{B} is the isotropic permeability of the medium. The first term within the parenthesis may be interpreted as a driving force arising from a pressure gradient and the second term represents a resisting force due to fluid viscosity. Now turning to interface flows, we have shown in Vernerey (2011) that for the case of isotropic interfaces, a Darcy-type relation can be established in terms of four macroscopic scalar permeabilities $\kappa_s^{\perp}$, $\kappa_s^{\parallel}$, $\kappa_m^{\perp}$, and $\kappa_m^{\parallel}$ such that:

$$q_s^{\perp} = -\frac{\kappa_s^{\perp}}{\mu}\frac{[p]}{2h} \quad q_s^{\parallel} = -\frac{\kappa_s^{\parallel}}{\mu}\{\nabla p\}^{\parallel} \tag{10}$$

$$q_m^{\perp} = -\frac{\kappa_m^{\perp}}{\mu}[\nabla p]^{\perp} \quad q_m^{\parallel} = -\frac{\kappa_m^{\parallel}}{\mu}[\nabla p]^{\parallel}. \tag{11}$$

We note here that the above permeabilities physically represent the resistance of the interface to flow; More specifically, the permeabilities $\kappa_s^{\perp}$ and $\kappa_s^{\parallel}$ provide a measure of the resistance of the interface to mean flow $\mathbf{q}_s$ (normally and tangentially, respectively), while $\kappa_m^{\perp}$ and $\kappa_m^{\parallel}$ are interpreted as the resistance of the interface to the first moment $\mathbf{q}_m$ of the interface flow distribution (normal and tangential components, respectively). However, at this point, there is no relationship between these permeabilities, the geometry and the nature of the material in the interface.

The next section intends to provide such a relationship by taking the following approach. Considering the microscopic problem of Darcy–Brinkman flow near a microscopic interface of finite thickness, we investigate the nature of microscopic interface fluxes in terms of various interface and bulk properties. The information gleaned from this study is then utilized in conjunction with the concept of thickness averaging so that a relationship between microscopic and macroscopic flows can be established. This subsequently enables the derivation of macroscopic permeabilities in terms of microscopic interface properties in Sect. 4.

3 Microscopic Darcy–Brinkman Flow Near an Interface

Locally, the interface is represented as a porous medium of finite thickness delimited by two boundaries located at $\xi_n = -h$ and $\xi_n = h$ in a local Cartesian coordinate system $\{\xi_t, \xi_n\}$ as shown in Fig. 3. The interface is surrounded by an infinite porous medium characterized by different properties. The microscopic velocity $\tilde{\mathbf{q}}$ is locally derived from the Darcy–Brinkman equation in terms of the pressure gradient ∇p as:

$$\mu_e \nabla^2 \tilde{\mathbf{q}} - \frac{\mu}{\kappa}\tilde{\mathbf{q}} - \nabla p = 0, \tag{12}$$

where the permeability κ, and the effective Brinkman viscosity μ_e are different in the interface and the bulk:

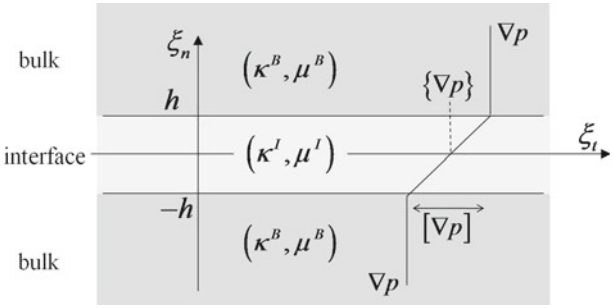

Fig. 3 Microscopic description of the interface of thickness $2h$

$$\{\kappa, \mu_e\} = \left\{\kappa^I, \mu_e^I\right\} \quad \xi_n \in [-h, h] \tag{13}$$

$$= \left\{\kappa^B, \mu_e^B\right\} \quad \xi_n \in]-\infty, -h[\cup]h, \infty[. \tag{14}$$

In addition, the pressure gradient profile in the interface may be written as a Taylor series around the center of the interface ($\xi_n = 0$) in terms of the macroscopic mean pressure gradient $\{\nabla p\}$ and the macroscopic jump in pressure gradient $[\nabla p]$ across Γ as:

$$\begin{aligned} \nabla p\,(\xi_n) &= \{\nabla p\} - \frac{[\nabla p]}{2} \quad \xi_n \in]-\infty, -h[\\ &= \{\nabla p\} + \frac{[\nabla p]}{2h}\xi_n + o\left(\xi_n^2\right) \quad \xi_n \in [-h, h] \\ &= \{\nabla p\} + \frac{[\nabla p]}{2} \quad \xi_n \in]h, \infty[\end{aligned} \tag{15}$$

Upon solving the microscopic flow $\tilde{\mathbf{q}}$ with (12), the macroscopic velocities $\mathbf{q}_s$ and $\mathbf{q}_m$ are found by the averaging operation:

$$\mathbf{q}_s = \frac{1}{2h}\int_{-h}^{h} \tilde{\mathbf{q}}(\xi_n)\mathrm{d}\xi_n, \quad \mathbf{q}_m = \frac{1}{(2h)^2}\int_{-h}^{h} \tilde{\mathbf{q}}(\xi_n)\xi_n\mathrm{d}\xi_n. \tag{16}$$

The perpendicular and tangential components of each velocity can then be obtained by projecting $\mathbf{q}_s$ and $\mathbf{q}_m$ along the normal $\mathbf{n}$ and in the plane of the interface, respectively. To simplify the general analysis, we propose to decouple the normal and tangential problems by projecting (12) onto a normal and tangential directions. This method will enable us to directly determine normal and tangential velocities in the interface as shown in the next section. Furthermore, we consider that the microscopic fluid velocity $\tilde{\mathbf{q}}$ varies linearly in the tangential direction near the interface :

$$\frac{\partial^2 \tilde{\mathbf{q}}}{\partial \xi_t^2} = 0. \tag{17}$$

This assumption will greatly simplify the equations presented below and does not affect the derivation of effective interface permeabilities presented at the end of this article.

3.1 Normal flow

To obtain an expression for the normal interface velocity $\tilde{q}_n$, we start by projecting (12) onto the normal direction $\mathbf{n}$; this yields:

$$-\frac{\mu}{\kappa^I}\tilde{q}_n - \frac{\partial p}{\partial \xi_n} = 0 \quad \xi_n \in [-h, h], \tag{18}$$

where Eq. (17) was invoked and we enforced $\partial^2 \tilde{q}_n / \partial \xi_n^2 = 0$ from the incompressibility assumption. In addition, projecting (15) in the normal direction leads to:

$$\frac{\partial p}{\partial \xi_n}(\xi_n) = \frac{[p]}{2h} + \frac{[\nabla p]^{\perp}}{2h}\xi_n + o\left(\xi_n^2\right) \quad \xi_n \in [-h, h], \tag{19}$$

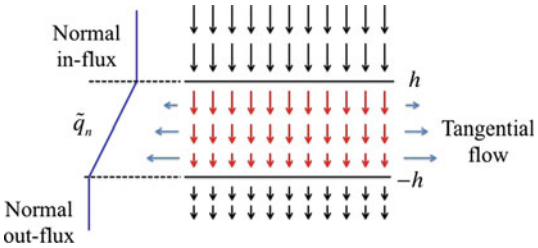

Fig. 4 Schematic displaying the change of normal flow through the interface. Note that for incompressible fluids, a variation of flow is only possible if tangential flow is allowed

where we used the fact that $\{\nabla p\}^{\perp} = [p]/2h$. Substituting (19) into (18) immediately leads to an expression for the normal interface velocity $\tilde{q}_n$:

$$\tilde{q}_n = -\frac{\kappa^I}{2\mu h}\left([p] + [\nabla p]^{\perp}\,\xi_n\right). \tag{20}$$

This expression shows that the normal velocity arises from a jump in pressure across the interface and exhibits a linear variation when a jump $[\nabla p]^{\perp}$ in pressure gradient is present. Note that in order to ensure that the condition of incompressibility at the microscale, one should verify that $\text{div}\tilde{\mathbf{q}} = \partial\tilde{q}_n/\partial\xi_n + \partial\tilde{q}_t/\partial\xi_t = 0$. Assessing the divergence with the help of Eq. (20) implies that the normal flow generates a tangential flow $\tilde{q}_t$ that varies in the tangential direction such that $\partial\tilde{q}_t/\partial\xi_t = -\frac{\kappa^I}{2\mu h}[\nabla p]^{\perp}$ (Fig. 4). This implies that if no tangential flow is allowed through the interface, the normal flow may not vary through the interface ($[\nabla p]^{\perp} = 0$). This phenomena is accounted for in the mass balance equation (6).

3.2 Tangential flow

The tangential component of the microscopic velocity $\tilde{q}_t$ may then be obtained by projecting (12) onto the tangential direction $\mathbf{t}$ as follows:

$$\mu_{\text{e}}\frac{\partial^2\tilde{q}_t}{\partial\xi_n^2} - \frac{\mu}{\kappa}\tilde{q}_t - \frac{\partial p}{\partial\xi_t} = 0, \tag{21}$$

where once again, the second derivative of $\tilde{q}_t$ with respect to ξ_t was set to zero (17). Furthermore, it can be shown that the pressure gradient $\partial p/\partial\xi_t$ is obtained by replacing $\{\nabla p\}$ by $\{\nabla p\}^{\|}$ and $[\nabla p]$ by $[\nabla p]^{\|}$ in expression (15). The equation may then be solved by assuming that the tangential velocity converges to a constant values far from the interface. This leads to the following far-field boundary conditions:

$$\frac{\partial\tilde{q}_t}{\partial\tilde{\xi}_n}(-\infty) = 0, \quad \frac{\partial\tilde{q}_t}{\partial\tilde{\xi}_n}(\infty) = 0. \tag{22}$$

Given the form of the pressure distribution and boundary conditions, the solution $\tilde{q}_t$ can be decomposed into a symmetric and antisymmetric solutions $\tilde{v}$ and $\tilde{w}$, respectively, such that $\tilde{q}_t = \tilde{v} + \tilde{w}$. It is also convenient to non-dimensionalize (21) by introducing characteristic velocities and length-scales as:

$$v^{\star} = \frac{\kappa^I\{\nabla p\}^{\|}}{\mu} \quad w^{\star} = \frac{\kappa^I[\nabla p]^{\|}}{2\mu} \quad \text{and} \quad \ell^{\star} = \sqrt{\frac{\kappa^I\mu_{\text{e}}^I}{\mu}} \tag{23}$$

such that the solutions can be written in terms of non-dimensional variables defined by:

$$\bar{v} = \frac{\tilde{v}}{v^\star}, \quad \bar{w} = \frac{\tilde{w}}{w^\star} \quad \text{and} \quad \bar{\xi}_n = \frac{y}{\ell^\star}. \tag{24}$$

For simplicity, we only consider the solution on $[0, \infty[$ since the domain $]-\infty, 0[$ may be recovered by symmetry. The variables $\bar{v}$ and $\bar{w}$ are solutions of the following two equations:

$$\frac{\partial^2 \bar{v}}{\partial \bar{\xi}_n^2} - \bar{v} - 1 = 0, \quad \frac{\partial^2 \bar{w}}{\partial \bar{\xi}_n^2} - \bar{w} - \frac{\bar{\xi}_n}{\bar{h}} = 0 \quad \bar{\xi}_n \in [0, \bar{h}] \tag{25}$$

$$\frac{\partial^2 \bar{v}}{\partial \bar{\xi}_n^2} - \alpha \bar{v} - \beta = 0, \quad \frac{\partial^2 \bar{w}}{\partial \bar{\xi}_n^2} - \alpha \bar{w} - \beta = 0 \quad \bar{\xi}_n \in [\bar{h}, \infty[, \tag{26}$$

which consist of the symmetric and antisymmetric parts of (21). In (25), we introduced the non-dimensional interface half-thickness $\bar{h} = h/\ell^\star$ and normalized interface properties β, γ, and α as:

$$\beta = \frac{\mu_{\mathrm{e}}^I}{\mu_{\mathrm{e}}^{\mathrm{B}}}, \quad \gamma = \frac{\kappa^I}{\kappa^{\mathrm{B}}} \quad \text{and} \quad \alpha = \beta\gamma \tag{27}$$

Due to the symmetry of $\bar{v}$ and antisymmetry of $\bar{w}$, the boundary conditions on $[0, \infty[$ can be rewritten:

$$\frac{\partial \bar{v}}{\partial \bar{\xi}_n}(0) = 0, \quad \frac{\partial \bar{v}}{\partial \bar{\xi}_n}(\infty) = 0, \quad \bar{w}(0) = 0, \quad \frac{\partial \bar{w}}{\partial \bar{\xi}_n}(\infty) = 0. \tag{28}$$

Furthermore, requiring continuity of both the velocity field and its derivative at the interface boundary $\xi_n = h$, we obtain the following matching conditions:

$$\lim_{\bar{\xi}_n \to \bar{h}^+} \bar{v}(\bar{\xi}_n) = \lim_{\bar{\xi}_n \to \bar{h}^-} \bar{v}(\bar{\xi}_n) \quad \lim_{\bar{\xi}_n \to \bar{h}^+} \frac{\partial \bar{v}}{\partial \bar{\xi}_n} = \lim_{\bar{\xi}_n \to \bar{h}^-} \frac{\partial \bar{v}}{\partial \bar{\xi}_n} \tag{29}$$

$$\lim_{\bar{\xi}_n \to \bar{h}^+} \bar{w}(\bar{\xi}_n) = \lim_{\bar{\xi}_n \to \bar{h}^-} \bar{w}(\bar{\xi}_n) \quad \lim_{\bar{\xi}_n \to \bar{h}^+} \frac{\partial \bar{w}}{\partial \bar{\xi}_n} = \lim_{\bar{\xi}_n \to \bar{h}^-} \frac{\partial \bar{w}}{\partial \bar{\xi}_n} \tag{30}$$

Upon solving these linear ordinary equations, the symmetric and antisymmetric solutions can be written in the form:

$$\bar{v}\left(\bar{\xi}_n\right) = -1 + (1 - A)\frac{\cosh(\bar{\xi}_n)}{\cosh(\bar{h})} \quad \bar{\xi}_n \in [0, \bar{h}] \tag{31}$$

$$= -\frac{1}{\gamma} + \left(\frac{1}{\gamma} - A\right) e^{\sqrt{\alpha}(\bar{h} - \bar{\xi}_n)} \quad \bar{\xi}_n \in [\bar{h}, \infty[\tag{32}$$

and

$$\bar{w}\left(\bar{\xi}_n\right) = -\frac{\bar{\xi}_n}{\bar{h}} + (1 - B)\frac{\sinh(\bar{\xi}_n)}{\sinh(\bar{h})} \quad \bar{\xi}_n \in [0, \bar{h}] \tag{33}$$

$$= -\frac{1}{\gamma} + \left(\frac{1}{\gamma} - B\right) e^{\sqrt{\alpha}(\bar{h} - \bar{\xi}_n)} \quad \bar{\xi}_n \in [\bar{h}, \infty[, \tag{34}$$

where the constants A and B are written in terms of $\bar{h}$, α, and β as:

$$A = \frac{\beta + \sqrt{\alpha}\tanh(\bar{h})}{\alpha + \sqrt{\alpha}\tanh(\bar{h})} \quad \text{and} \quad B = \frac{\beta\bar{h} - \sqrt{\alpha} + \sqrt{\alpha}\bar{h}\coth(\bar{h})}{\bar{h}\left(\alpha + \sqrt{\alpha}\coth(\bar{h})\right)}$$

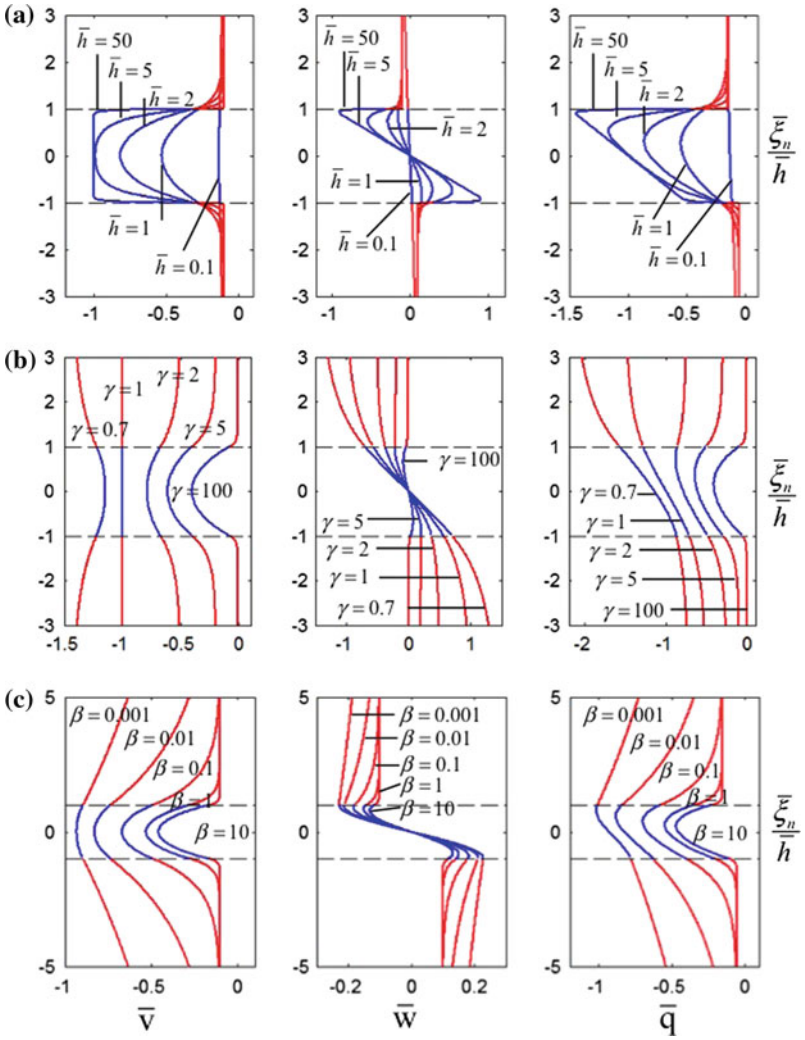

Fig. 5 **a** Effect of interface thickness on tangential flow at $\gamma = 10$ and $\beta = 1$. **b** Effect of interface permeability on tangential flow at $\bar{h} = 1$ and $\beta = 1$. **c** Effect of effective viscosity on tangential flow at $\bar{h} = 1$ and $\gamma = 10$

The final solution $\tilde{q}_t$ is subsequently written as a combination of $\bar{v}$ and $\bar{w}$ as:

$$\tilde{q}_t = \frac{\kappa^I}{\mu}\left(\bar{v}\{\nabla p\}^{\parallel} + \bar{w}\frac{[\nabla p]^{\parallel}}{2}\right). \tag{35}$$

It can be seen that the nature of the interface tangential flow mainly depends on three parameters that consists of $\bar{h}$, β and γ as depicted in Fig. 5. It is first important to note that interface thickness is defined in relation to the length-scale defined by $\sqrt{\kappa^I \mu_e^I/\mu}$. In other words, a given value of h may be considered small for a highly viscous fluid and a small interface permeability, while it may be considered large in the opposite situation. Figure 5a shows the nondimensional tangential velocities for different values of $\bar{h}$ when $\gamma = 10$ and $\beta = 1$. Generally, the figure shows that for small values of $\bar{h}$, the interface dimensions are

too small in order for the tangential flow to fully develop independently from the bulk flow. However, as $\bar{h}$ increases to values close to unity, interface flow starts developing but is still constrained by a transition zone between bulk and interface. However, as $\bar{h}$ increases to larger values, the characteristic length of the transition dramatically reduces such that interface and bulk flows become quasi independent at $\bar{h} = 50$. These observations are valid for both the symmetric and antisymmetric parts of the flows, which implies that the development of both the mean and first moment of interface flow are promoted by large values of $\bar{h}$.

The effect of interface permeability, characterized by the ratio $\gamma = \kappa^I/\kappa^{\mathrm{B}}$ is also illustrated in Fig. 5b for constant interface thickness ($\bar{h} = 1$) and effective viscosity ratio ($\beta = 1$). As expected, interface flow is slower in the interface for $\gamma < 1$ and faster for $\gamma > 1$. In addition, as γ increases, the first moment of interface flow can fully develop in the interface, which triggers a sharp flow discontinuity across the interface. However, as γ decreases below unity, the interface becomes more resistant to bfq_m and the transition region (or boundary layer) mostly occurs in the bulk.

Similarly, the effective viscosity ratio $\beta = \mu_{\mathrm{e}}^I/\mu_{\mathrm{e}}^{\mathrm{B}}$ plays a large influence on the extend of the boundary layer near the interface as shown in Fig. 5c. Generally, the extent of the influence of interface flow on bulk flow increases with decreasing β (or increasing bulk viscosity $\mu_{\mathrm{e}}^{\mathrm{B}}$).

4 Macroscopic Permeabilities and Their Relation to Microscopic Interface Properties

To bridge micro and macroscopic interface descriptions, we now seek to express macroscopic permeabilities introduced in (10) and (11) in terms of interface properties $\bar{h}$, γ, and β. This may be accomplished by projecting the averaging operation defined in (16) along the normal and tangential interface directions and identifying the velocity-pressure relation with (10) and (11).

4.1 Normal permeabilities

Normal macroscopic permeabilities are obtained by projecting (16) onto the normal direction. This yields:

$$q_s^{\perp} = \frac{1}{2h}\int_{-h}^{h} \tilde{q}_n d\xi_n = -\frac{\kappa^I\,[p]}{2\mu h} \tag{36}$$

$$q_m^{\perp} = \frac{1}{4h^2}\int_{-h}^{h} \tilde{q}_n \xi_n d\xi_n = -\frac{\kappa^I I\,[\nabla p]^{\perp}}{\mu}, \tag{37}$$

where we used (20) to obtain the last terms. Identifying these expressions with (10) and (11) leads to:

$$\bar{\kappa}_s^{\perp} = 1 \quad \text{and} \quad \bar{\kappa}_m^{\perp} = I, \tag{38}$$

where I was defined in (8), and the above permeabilities are normalized with respect to interface permeability κ^I, i.e., $\bar{\kappa}_s^{\perp} = \kappa_s^{\perp}/\kappa^I$ and $\bar{\kappa}_m^{\perp} = \kappa_m^{\perp}/\kappa^I$. These results show that normal interface permeabilities are entirely expressed in terms of the microscopic permeability κ^I and are independent of the interface thickness h. This is expected as the fluid viscosity, which gives rise to size effects, does not play a role in the normal direction.

4.2 Tangential permeabilities

In turn, macroscopic tangential permeabilities are obtained by projecting (16) onto the tangential direction as follows:

$$q_s^{\parallel} = \frac{1}{2h}\int_{-h}^{h} \tilde{q}_t \mathrm{d}\xi_n = \frac{\kappa_I \{\nabla p\}^{\parallel}}{2\bar{h}\mu} \int_{-\bar{h}}^{\bar{h}} \bar{v}\, \mathrm{d}\bar{\xi}_n \tag{39}$$

$$q_m^{\parallel} = \frac{1}{4h^2}\int_{-h}^{h} \tilde{q}_t \xi_n \mathrm{d}\xi_n = \frac{\kappa_I [\nabla p]^{\parallel}}{8\bar{h}^2\mu} \int_{-\bar{h}}^{\bar{h}} \bar{w}\bar{\xi}_n\, \mathrm{d}\bar{\xi}_n, \tag{40}$$

where we implicitly used the expression for $\tilde{q}_t$ in (35). Identifying the above equations with (10) and (11), the macroscopic permeabilities are found to be the zeroth and first moment of the symmetric and antisymmetric nondimensional velocities $\bar{v}$ and $\bar{w}$ in the interface, respectively:

$$\bar{\kappa}_s^{\parallel} = -\frac{1}{2\bar{h}}\int_{-\bar{h}}^{\bar{h}} \bar{v}\mathrm{d}\bar{\xi}_n \quad \text{and} \quad \bar{\kappa}_m^{\parallel} = -\frac{1}{8\bar{h}^2}\int_{-\bar{h}}^{\bar{h}} \bar{w}\bar{\xi}_n \mathrm{d}\bar{\xi}_n. \tag{41}$$

Substituting (31) and (33) into (41) and performing the integration yields the following forms for the mean tangential permeability:

$$\bar{\kappa}_s^{\parallel} = 1 - \frac{\beta\,(\gamma - 1)\tanh(\bar{h})}{\bar{h}\left(\alpha + \sqrt{\alpha}\tanh(\bar{h})\right)} \tag{42}$$

and the tangential permeability to the first moment of interface flow:

$$\bar{\kappa}_m^{\parallel} = I - \frac{\left(\bar{h}\beta\,(\gamma - 1) - \sqrt{\alpha}\right)\left(\bar{h}\coth(\bar{h}) - 1\right)}{4\bar{h}^3(\alpha + \sqrt{\alpha}\coth(\bar{h}))}. \tag{43}$$

These two relationships, together with (38) are the main results of this article. They indeed provide a clear relation between macroscopic permeabilities and microscopic interface parameters. To better understand these findings, Fig. 6 provides an illustration of the variation of macroscopic tangential permeabilities in terms of changes in microscopic interface properties. Thus, Fig. 6a shows that mean permeability $\kappa_s^{\parallel}$ varies nonlinearly from being equal to the bulk permeability κ^{B} when $\bar{h} = 0$, to being equal to the interface permeability κ^I when $\bar{h}$ becomes large compared to unity. Similarly, the permeability $\bar{\kappa}_m^{\parallel}$ varies from 0 when $\bar{h} = 0$, to $I\kappa^I$ for large values of $\bar{h}$. In other words, thin interfaces ($\bar{h} \to 0$) tend to prohibit any flow $q_m^{\parallel}$ in comparison to thicker ones. An interesting feature is the existence of an optimum value of $\bar{h}$ (around 1) for which $\kappa_m^{\parallel}$ reaches a maximum when $\gamma < 1$. This phenomenon may be explained as follows; for large values of $\bar{h}$, interface flow is totally independent from that in the bulk and the value of $\kappa_m^{\parallel}$ approaches that of an infinitely thick interface $\kappa_m^{\parallel} = I\kappa^I$. However, when $\bar{h} \approx 1$, significant interactions exist between bulk flow and interface flow; the fast bulk flow tends to increase the first moment of interface fluid velocity in the interface due to viscous interactions (right figure in Fig. 6a). The consequence is an increased value of $\kappa_m^{\parallel}$ for intermediate values of $\bar{h}$.

The influence of interface permeability ratio γ is then assessed on macroscopic properties as depicted in Fig. 6b. Results show that both $\kappa_s^{\parallel}$ and $\kappa_m^{\parallel}$ are decreasing functions of γ.

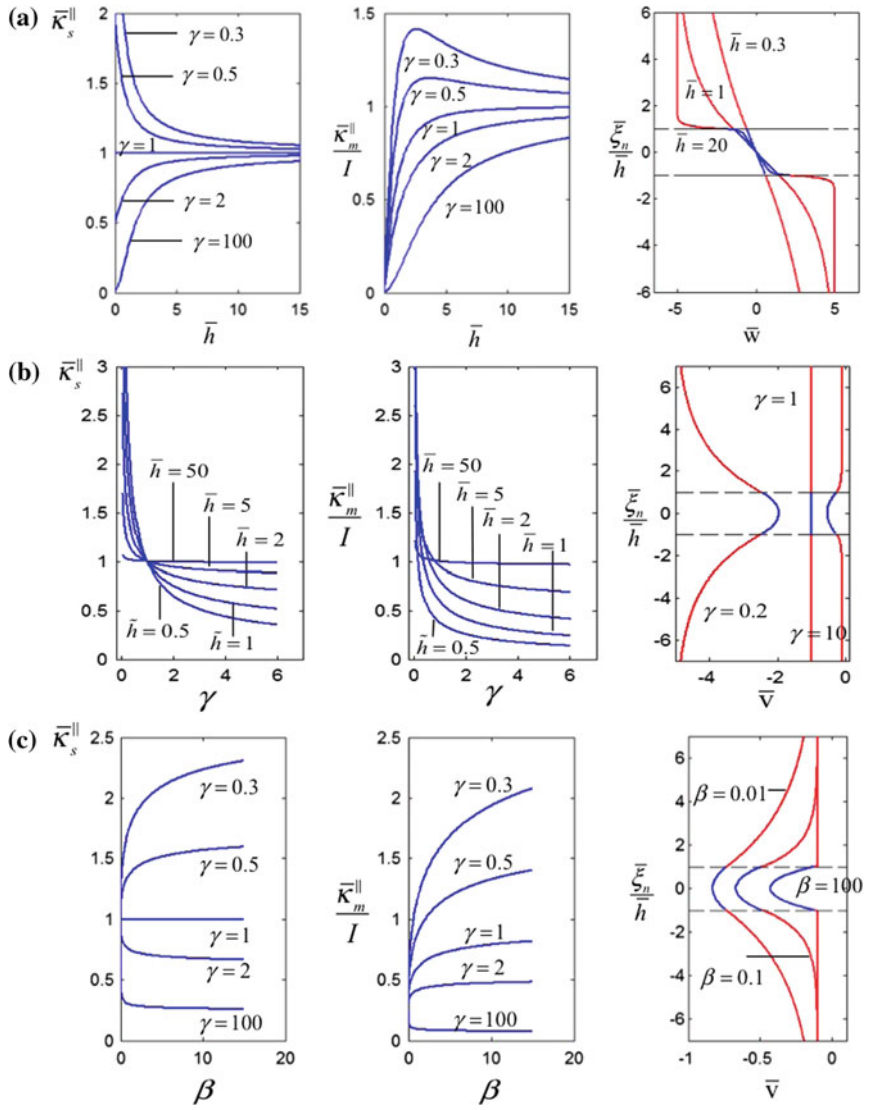

Fig. 6 **a** Effect of interface thickness effective permeabilities $\bar{\kappa}_s^{\parallel}$ and $\bar{\kappa}_m^{\parallel}$. For all cases, $\beta = 1$. Note that the permeability $\bar{\kappa}_m^{\parallel}$ exhibits a maximum around $\bar{h} = 1$ when $\gamma < 1$. This can be explained in terms of velocity ratios as shown in the last figure for $\gamma = 0.2$ and $\beta = 1$. It can clearly be seen that the maximum flow $q_m^{\parallel}$ is observed when $\bar{h} = 1$. **b** Effect of permeability ratio γ on effective permeabilities. For all cases, $\beta = 1$. **c** Effect of viscosity ratio β on effective permeabilities. For all cases, $\beta = 1$

When $\gamma > 1$, mean interface velocity is decreased by the slower bulk velocity due to viscous interactions as shown in the last figure of Fig. 6b. This phenomenon tends to decrease the mean tangential permeability. The opposite effect can be observed when $\gamma < 1$. In this case, bulk velocity is larger than interface velocity and this tends to increase tangential permeabilities. It should be noted that as the interface thickness becomes larger, these interactions become negligible as dragging effects between bulk and interface vanish. This explains why

for large thickness ($\bar{h} \to \infty$), the curves converges to horizontal lines corresponding to $\kappa_s^{\parallel} = \kappa^I$ and $\kappa_m^{\parallel} = I\kappa^I$.

Finally, Fig. 6c illustrates the role of permeability ratio $\beta = \mu_{\mathrm{e}}^I/\mu_{\mathrm{e}}^{\mathrm{B}}$ on bulk/interface interactions. Generally, as β increases, the effect of bulk velocity on interface permeabilities becomes more and more pronounced. This generally tends to increase $\kappa_{\parallel}$ when $\gamma < 1$ (i.e., when bulk velocity is larger than interface velocity) and decrease $\kappa_{\parallel}$ when $\gamma > 1$ (i.e., when bulk velocity is smaller than interface velocity).

5 Concluding Remarks

In summary, this article proposed to investigate the macroscopic properties of interfaces in porous media in terms of the microscopic properties, including thickness, permeability, and effective Brinkman viscosity. In particular, the major contribution of this work was to analytically derive relationships between interface permeabilities and microscopic properties and features in the context of the incompressibility and isotropy of the fluid and porous medium. We found that macroscopic tangential permeabilities are strongly affected by boundary layers developing at the boundary between bulk and interface domains. The size and nature of these layers were in turn strongly affected by interface thickness, permeability and effective viscosity. More specific findings can be stated as follows:

- The normal permeabilities are independent of interface thickness and only depend on the microscopic interface permeabililty κ^I.
- The mean tangential permeability is bounded between bulk permeability (for very thin interfaces) and interface permeability κ^I (for thick interfaces).
- The tangential permeability to the first moment of interface velocity varies between zero (for very thin interfaces) and $I\kappa^I$ (for thick interfaces). However, it reaches a maximum around $\bar{h} = 1$, in the case where $\kappa^I < \kappa^{\mathrm{B}}$.

In addition to providing a better understanding of fluid flow in porous interfaces, results reported in this article will enable the macroscopic modeling of interfaces in porous media as line discontinuity of zero thickness while keeping an accurate description of the microscopic properties through interface permeability definitions. This capability will prove useful in a variety of problems including soils mechanics, the mechanics of fractured porous media, fluid flow in biological media with interfaces and the mechanics of biological cells (Vernerey and Farsad 2011a; Farsad et al. 2010).

Acknowledgments The author gratefully acknowledges the National Science Foundation, Grant No. CMMI-0900607 and the National Institute of Health, Grant No. 1R21AR061011 in support of this work.

References

Barthelemym, J.F.: Effective permeability of media with a dense network of long and micro fractures. Transp. Porous Media **76**, 153–178 (2009)

Biot, M.A.: General theory of three-dimensional consolidation. J. Appl. Phys. **12**, 155–164 (1941)

Biot, M.A.: The elastic coefficients of the theory of consolidation. J. Astrophys. Astron **24**, 594–601 (1957)

Bowen, R.M.: Incompressible porous media models by the use of the theory of mixtures. Int. J. Eng. Sci. **18**, 1129–1148 (1980)

Chandesris, M., Jamet, D.: Boundary conditions at a planar fluid–porous interface for a poiseuille flow. Int. J. Heat Mass Transf. **49**(13–14), 2137–2150 (2006)

Dormieux, L., Kondo, D.: Approche micromecanique du couplage permeabilite-endommagement. Comptes Rendus Mecanique **332**, 135–140 (2007)
Farsad, M., Vernerey, F.J., Park, H.: An extended finite element/level set method to study surface effects on the mechanical behavior and properties of nanomaterials. Int. J. Numer. Methods Eng. **84**, 1466–1489 (2010)
Ghabezloo, S., Pouya, A.: Numerical upscaling of the permeability of a randomly cracked porous medium. In: The 12th International Conference of International Association for Computer Methods and Advances in Geomechanics (IACMAG) (2008)
Goyeaua, B., Lhuillierb, D., Gobina, G., Velardec, M.: Momentum transport at a fluid–porous interface. Int. J. Heat Mass Transf. **46**(21), 4071–4081 (2003)
Gurtin, M.E., Weissmuller, J., Larche, F.: A general theory of curved deformable interfaces in solids at equilibrium. Philos. Mag. A **78**, 1093–1109 (1998)
Liolios, P.A., Exadaktylos, G.E.: A solution of steady-state fluid flow in multiply fractured isotropic porous media. Int. J. Solids Struct. **43**, 3960–3982 (2008)
Pouya, A., Ghabezloo, S.: Flow-stress coupled permeability tensor for fractured rock masses. Transp. Porous Media **32**, 1289–1309 (2008)
Sun, D.N., Gu, W.Y., Guo, X.E., Lai, W.M., Mow, V.C.: A mixed finite element formulation of triphasic mechano-electromechanical theory for charged, hydrated biological soft tissues. Int. J. Numer. Methods Eng. **45**, 1375–1402 (1999)
Truesdell, C.: Rational Thermodynamics. McGraw-Hill Series in Modern Applied Mathematics. McGraw-Hill, New York (1969)
Vernerey, F.J.: On the mechanics of interfaces in deformable porous media. Int. J. Solids Struct. doi:10.1016/j.ijsolstr.2011.07.005 (2011)
Vernerey, F.J., Farsad, M.: A constrained mixture approach to mechano-sensing and force generation in contractile cells. J. Mech. Behav. Biomed. Mater. doi:10.1016/j.jmbbm.2011.05.022 (2011a)
Vernerey, F.J., Farsad, M.: An eulerian/xfem formulation for the large deformation of cortical cell membrane. Comput. Methods Biomech. Biomed. Eng. **14**, 433–445 (2011b)
Vernerey, F.J., Foucard, L., Farsad, M.: Bridging the scales to explore cellular adaptation and remodeling. Bionanoscience. doi:10.1007/s12668-011-0013-6 (2011a)
Vernerey, F.J., Greenwald, E., Bryant, S.J.: Triphasic mixture model of cell-mediated enzymatic degradation of hydrogels. Comput. Methods Biomech. Biomed. Eng. doi:10.1080/10255842.2011.585973 (2011b)